

DESY Summer Student Program 2009

In-situ Observation of Drying Kinetics in Colloidal Thin Films

Suttipong Wannapaiboon

Chiang Mai University, Thailand

Dr. Stephan V. Roth

Dr. Mottakin M. Abul Kasham

Supervisor

21th July – 10th September 2009

Contents

Abstract	2
1. Introduction	3
1.1 Colloidal thin films	3
1.2 GISAXS at beamline BW4	3
2. Experimental	5
2.1 Sample preparation	5
2.2 Optical microscopy	6
2.3 GISAXS measurement	7
2.4 GISAXS data analysis	7
3. Results and discussion	9
3.1 Optical micrographs	9
3.2 GISAXS	13
4. Conclusion	18
5. Acknowledgements	18
6. References	19

In-situ Observation of Drying Kinetics in Colloidal Thin Films

Suttipong Wannapaiboon^a, Mottakin M. Abul Kashem^b, Stephan V. Roth^b

^a *Summer Student; Department of Chemistry, Faculty of Science, Chiang Mai University, Chiang Mai 50200, Thailand*

^b *HASYLAB, DESY, Notkestrasse 85, D-22607 Hamburg, Germany*

Abstract

Driven by noteworthy applications of homogeneous and controllable structure of polymer thin films, the in-situ observation of drying kinetics in colloidal thin films has been investigated. During this summer student program, I have practiced and studied the drying process of colloidal polystyrene solutions and the characterization of the structure of polystyrene thin films by using optical microscopy and grazing incidence small-angle X-ray scattering technique. It is revealed that the drying kinetics process can be explained by the driving of the convective flow due to the evaporating of solvent in the droplets which therefore transports the particles and follow-up drying process from the center to the periphery of the droplet. The influences of preparative parameters such as concentration of colloidal polystyrene solutions, particles size and surface of substrate on the structure of dried droplets have been investigated. The GISAXS data informs the structures of polystyrene thin films, the composition of form factor and structural factor of the intensity and the thickness of the polystyrene thin film.

1. Introduction

1.1 Colloidal thin films

Driven by noteworthy applications, the creation of colloidal polymer thin films have been interest for years. For example, they are of interest in magnetic applications or for optical devices [1,2]. The materials used range from noble and magnetic metals to polymer nanoparticles. Due to the high demand on homogeneous areas and controllable structure, size and growth direction of polymer thin films, many basic researches based on structural studies have been conducted [3]. In order to produce the useful polymer thin films, it is necessary to understand the drying kinetics process and the influences of preparative parameters on thin film structures. Therefore, we are interested in the in-situ observation of drying kinetics in colloidal thin films. Moreover, if we can control the production of polymer thin films, they can be used as a template for patterning of hard inorganic materials such as metal nanoparticles. The advantage of a polymer template is the easy process ability and low-cost fabrications to produce the ordered pattern as well as, controllable size and localization of metal nanoparticles [4]. The deposition of metal nanoparticles such as gold nanoparticles on solid surfaces in an ordered pattern with controllable size and dispersion can serve various applications in nanoelectronics, nanocatalysts, bioelectronics, magnetic recording devices and gas sensors [1,5,6].

1.2 GISAXS at beamline BW4

The beamline BW4 of the DORIS III storage ring at HASYLAB, DESY has been designed as a small-angle X-ray scattering instrument. Due to its wiggler generated beam with high flux and excellent collimation, analysis of this scattering data provides the high resolution of structural information which can be length scales of some ten to several hundred

nanometers. The beamline layout is schematically shown in Figure 1[7]. Small-angle X-ray scattering is a very powerful tool for material characterization, especially for bulk samples by using transmission geometry. However, in the cases that the thin film sample on substrate or only the microstructure on the surface are of interest, the transmission mode is not appropriate due to the low scattering power of the thin film. Therefore, the grazing incidence small-angle X-ray scattering or GISAXS is used instead [8]. The schematic view of GISAXS measurement is illustrated in Figure 2. The sample surface is placed horizontally compared to the beam direction. The sample is mounted on a full 3-circle-goniometer and an x/y/z translation stage in order to change the measurement to reflection mode. GISAXS yields the surface sensitivity which enables the investigation of surfaces and thin films down to the sub-molecular range. One valuable advantage of GISAXS over SAXS is the improvement of resolution limit. Due to the reflection, the direct beam is well separated from the diffuse scattering. The direct as well as the specular reflected beam are blocked by two separate point-like beamstops. Therefore very small values of scattering vector q can be observed. There are several of structural studies of very thin layers by using GISAXS measurement such as semiconductor nanostructures (quantum dots, nanowires, nanotubes and nanolayers), nanocomposite thin films, micro-domain formation and ordering in polymer thin films [8-10].

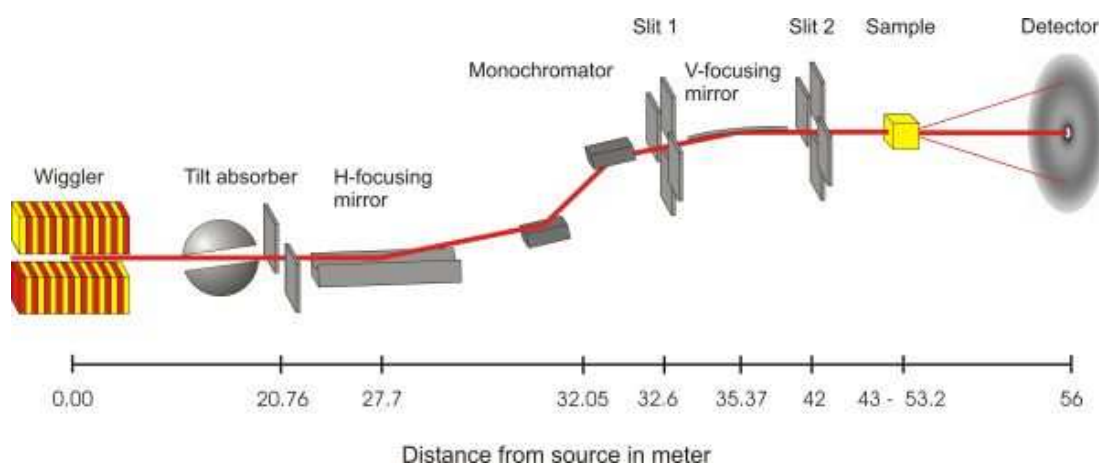


Figure 1 The layout of BW4 beamline instrument [7]

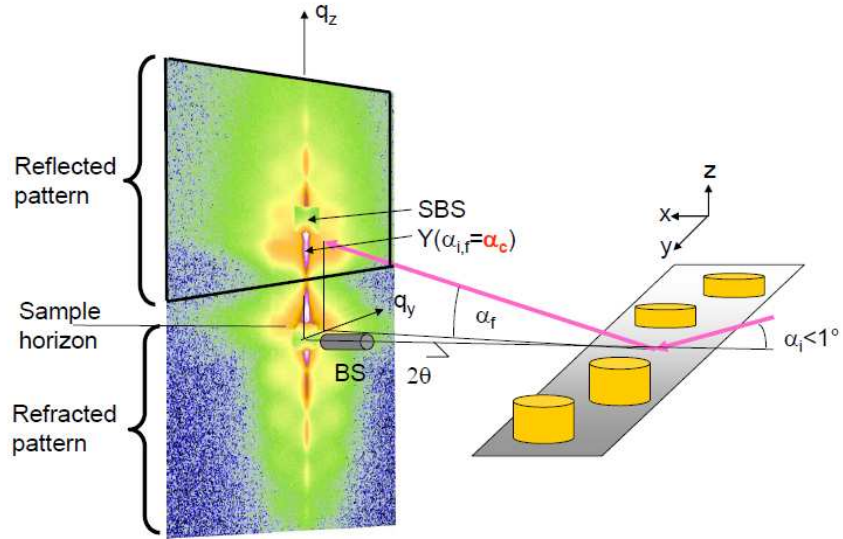


Figure 2 The schematic view of GISAXS measurement

2. Experimental

2.1 Sample preparation

Polystyrene colloidal thin films were prepared on top of Si(100) surface, covered with its native oxide layer. Firstly, the Si substrates ($2.5 \times 2.5 \text{ cm}^2$) were cleaned as follows in two ways:

- 1) Soaking in isopropanol for 30 min, shaking in another isopropanol solution for 5 min, and acetone-rinsing for 2 min. The cleaned substrate were further rinsed in deionized water for 2 min to remove the organic residues. Finally, the oil-free nitrogen gas was used for drying.
- 2) The additional cleaning step by using 19% w/w hydrofluoric acid solution for 2 min was used to remove the native silicon oxide layer for some case.

A polystyrene film with a nominal, thickness of 90 nm, was coated on top of Si substrate in order to prepare hydrophobic surface. In order to prepare colloidal polystyrene thin films, various polystyrene colloidal particle solutions were deposited by pipette on top of cleaned Si substrate and dried at room temperature. The droplets had a diameter about 0.5

cm. The code of sample and the variation of preparative parameters for preparing polystyrene thin films were listed as follows;

(L or without L) + A, B, C + 1 - 8 + PSXX + 2ul, 5ul, 10ul

- L polystyrene colloidal particle size 384 nm
 Without L polystyrene colloidal particle size 96 nm
- A, B, C type of Si substrates which were cleaned the surface with
 A HF solution to remove native silicon oxide layer
 B only isopropanol and acetone
 C Si substrate with polystyrene coating
- 1 – 8 concentration of polystyrene colloidal particles
 1 --- 25 mg/ml 2 --- 10 mg/ml 3 --- 5.0 mg/ml
 4 --- 2.5 mg/ml 5 --- 1.0 mg/ml 6 --- 0.50 mg/ml
 7 --- 0.10 mg/ml 8 --- 0.050 mg/ml
- PSXX number of sample droplets
- 2ul, 5ul, 10ul volume of droplets

The samples were further investigated using optical microscopy and GISAXS.

2.2 Optical microscopy

The optical microscope (Keyence VHX-600 series) with magnifications from x50 to x500 was used to study in-situ observation solution drying at room temperature. To do so, video files were made to follow the drying of polystyrene droplets. After finishing of the drying process, the optical micrographs of the structure of thin films were recorded. The drying kinetics process of polystyrene solutions was investigated from the video files and the optical micrographs. The interesting droplets, which formed homogeneous areas and line structures as observed from optical micrographs, were selected to GISAXS measurements.

2.3 GISAXS measurements

All GISAXS measurements were carried out at the beamline BW4 of the DORIS III storage ring at HASYLAB, DESY with the μ GISAXS set-up during the exercise week. The set-up parameters for GISAXS measurements were listed as follow;

- sample-to-detector distance 2.21 m
- wavelength of X-ray beam 0.138 nm
- pixel size of MARCCD detector 79.1 μm x 79.1 μm
- incidence angle $\alpha_i=0.3 - 0.5^\circ$

The sample was placed horizontally on the sample holder and scanned in the y-and α_i -direction aligning the sample surface horizontal to the beam, followed by the x-direction to make sure that the sample is aligned. The direct beam was blocked by using a diode beam-stop in between the sample and the detector to protect the detector from high intensity beam. Either a movable rod-like or point-like specular beam-stop was used. Sample measurement was started by supply the acquisition time by programming command and checked the highest intensity before making a CCD recording of data which will not saturate the CCD camera. The incident angle is always chosen to be higher than the critical angle of the polymer under investigation for penetrating the beam through the full depth of thin films. Therefore, the information of the interface correlations can be investigated from the resonance diffuse scattering (RDS).

2.4 GISAXS data analysis

The scattering patterns from GISAXS measurements were recorded on 2D MARCCD detector. The program “Fid2D” (<http://www.esrf.eu/computing/scientific/FIT2D/>) was used to analyze the two-dimensional GISAXS data. Instead of using the complete two-dimensional pattern, the cuts in horizontal and vertical direction were applied. The horizontal slices at

constant q_z are called *out-of-plane cuts* and the vertical slices at constant q_y are called *vertical cuts* which are named *detector scan* for vertical cut at $q_y=0$ and off-detector scans for vertical cuts at $q_y \neq 0$. The components of scattering vector (q) can be defined as follow;

$q_x = 2\pi(\cos\psi\cos\alpha_f - \cos\alpha_i)/\lambda$, $q_y = 2\pi(\sin\psi\cos\alpha_f)/\lambda$ and $q_z = 2\pi(\sin\alpha_i + \sin\alpha_f)/\lambda$ where α_i , α_f and ψ are incident angle, exit angle and out-of-plane angle, respectively. In this research, the out-of-plane cut at the position of Yoneda peak at pixel position $Y=880$ and the vertical cut at pixel position $X=1024$ were selected to explain the structure of polystyrene thin films.

The out-of-plane cuts which illustrate the intensity with respect to the position in columns of the detector are changed into the angular space representation by converting the columns pixel number to out-of-plane angle. The out-of-plane angle can define from the arctangent of distance between the center of symmetry and pixel position (D_{st}) divided by sample to detector distance (D_{SD}) as shown in the following equation;

$$\psi = \tan^{-1} \frac{D_{st}}{D_{SD}} = \tan^{-1} \frac{\text{pixel distance} \times \text{pixel size}}{D_{SD}} \quad \text{Eq. 1}$$

Moreover, a double logarithmic plot of intensity versus scattering vector component q_y is directly used for the determination of the structural information. Based on the reciprocal space representation, the part of intensity can be classified into form factor and structure factor by comparing this out-of-plane cut with the form factor of the sample particles. The form factor of spherical particles is illustrated in the following equation;

$$P(q_y) = \left[\frac{\sin(q_y r) - q_y r \cos(q_y r)}{(q_y r)^3} \right]^2 \quad \text{Eq. 2}$$

The length scales (ξ) of a structure factor can be calculated from q_y values at the peak positions in out-of-plane reciprocal space representation as $\xi = 2\pi / q_y$.

The vertical cuts are also illustrated in the angular space representation of intensity versus the sum of incident angle and exit angle ($\varphi = \alpha_i + \alpha_f$). The position of specular peak at $\varphi = 2\alpha_i$ and Yoneda peak at $\varphi = \alpha_i + \alpha_c$ can be observed from the vertical cut. The

thickness of thin films (d) can be calculated from two maxima adjacent peaks in the vertical cut as illustrated in the following equation;

$$d = \frac{\lambda}{\sin \alpha_{f,m} - \sin \alpha_{f,n}} \text{ with } m = n+1 \quad \text{Eq. 3}$$

3. Results and discussion

3.1 Optical micrographs

According to the recorded video files of the drying of colloidal polystyrene droplets, the drying kinetic process can be explained in a general way as follow. The evaporation of the solvent increases the concentration of colloidal polystyrene particles and consequently drives the convective flow in the droplets [11]. Therefore, the transportation of the particles and the follow-up drying from the center to the periphery of the droplet can be observed. However, the difference preparative parameters such as concentration of polystyrene solutions, particles size and type of substrate surfaces influence on the structure of the final dried droplets and the drying kinetics process. The optical micrographs of the final dried droplets as illustrated in Figure 3 indicate the influence of the concentration of polystyrene solutions on the structure of dried droplets in both the rim and the center parts. The pattern formation and the thickness of the polystyrene thin films in various areas inside the droplet are extremely controlled by this parameter. The decreasing concentration leads to small rim of the polystyrene film as shown in Figure 3(a) to 3(d). Additionally, gradual shrinkage of the droplets before they become completely dried can be examined in the case of the concentrations of the colloidal polystyrene solutions are equal or less than 1.0 mg/ml. The homogeneous line structure of polystyrene film in the middle of the droplet can be observed when the concentration of polystyrene solution is 0.50 mg/ml for only the case of particles size of polystyrene colloid is 384 nm as shown in Figure 3(f).

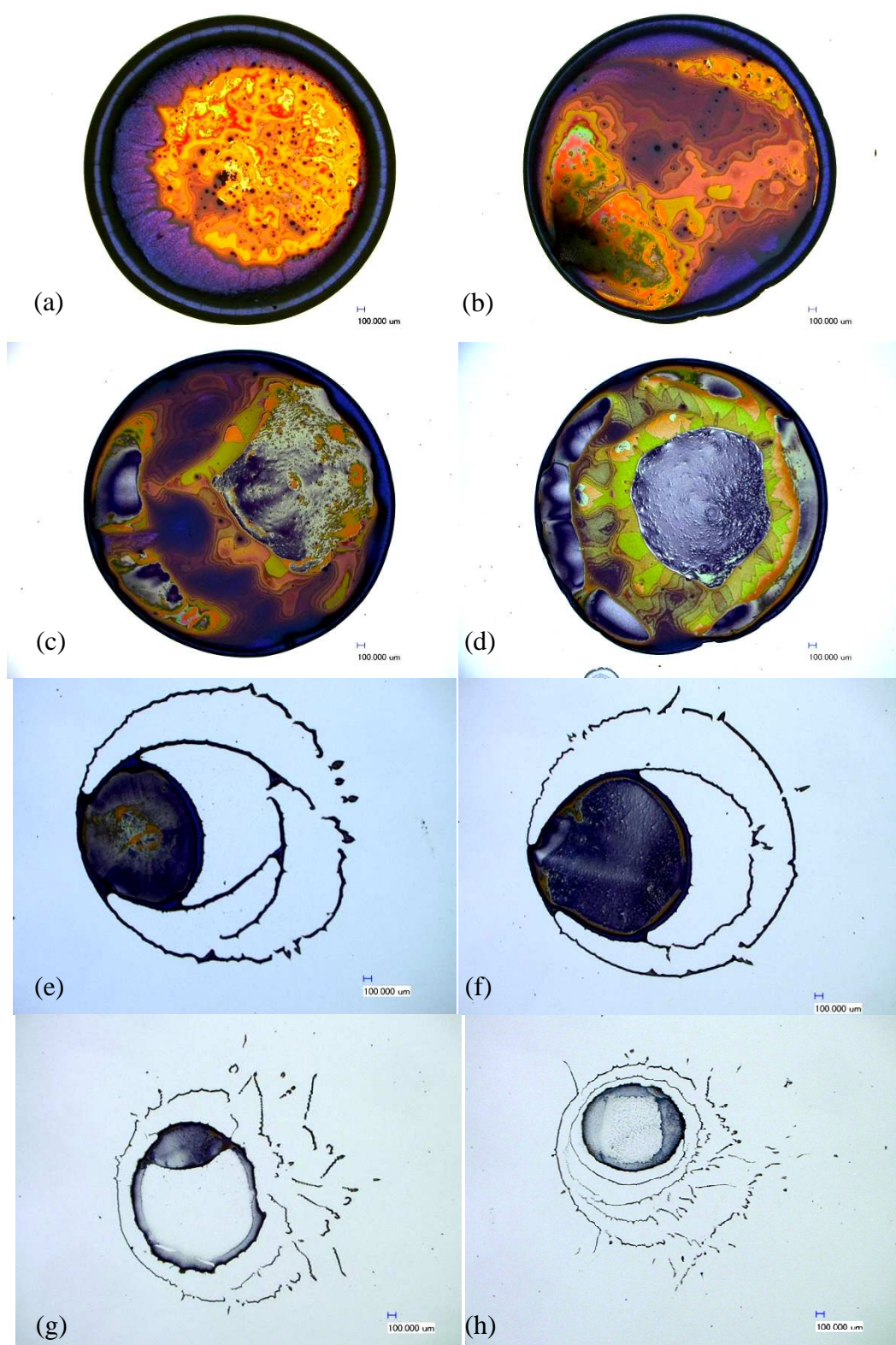


Figure 3 The x50 magnification optical micrographs of the final dried droplets from the polystyrene solutions with particles size 384 nm of the various concentrations (a) 25, (b) 10, (c) 5.0, (d) 2.5, (e) 1.0, (f) 0.50, (g) 0.10 and (h) 0.050 mg/ml on the Si substrates which were only cleaned by isopropanol and acetone

The x500 magnification optical micrographs as illustrated in Figure 4 show the influence of colloidal polystyrene particles size on the structures at the rim and the middle of the final dried droplets. The alteration of particles size from 96 nm to 384 nm (from Figure 4(a) to 4(b)) considerably shows the different patterns of the polystyrene colloidal thin films. It can be noteworthy that the line structural patterns at the rim positions can be generally observed only in the case of using colloidal polystyrene particles size of 96 nm. These line patterns can be distinctly indicated when using 10 mg/ml of colloidal polystyrene solution as shown in Figure 4(a). However, the drying of the bigger colloidal polystyrene particles does not generate the line patterns at the rim positions and therefore only the formation of the polystyrene thick films by the aggregation of the colloidal particles can be observed. The structures of the polystyrene films in the middle of droplets also show different patterns in both cases.

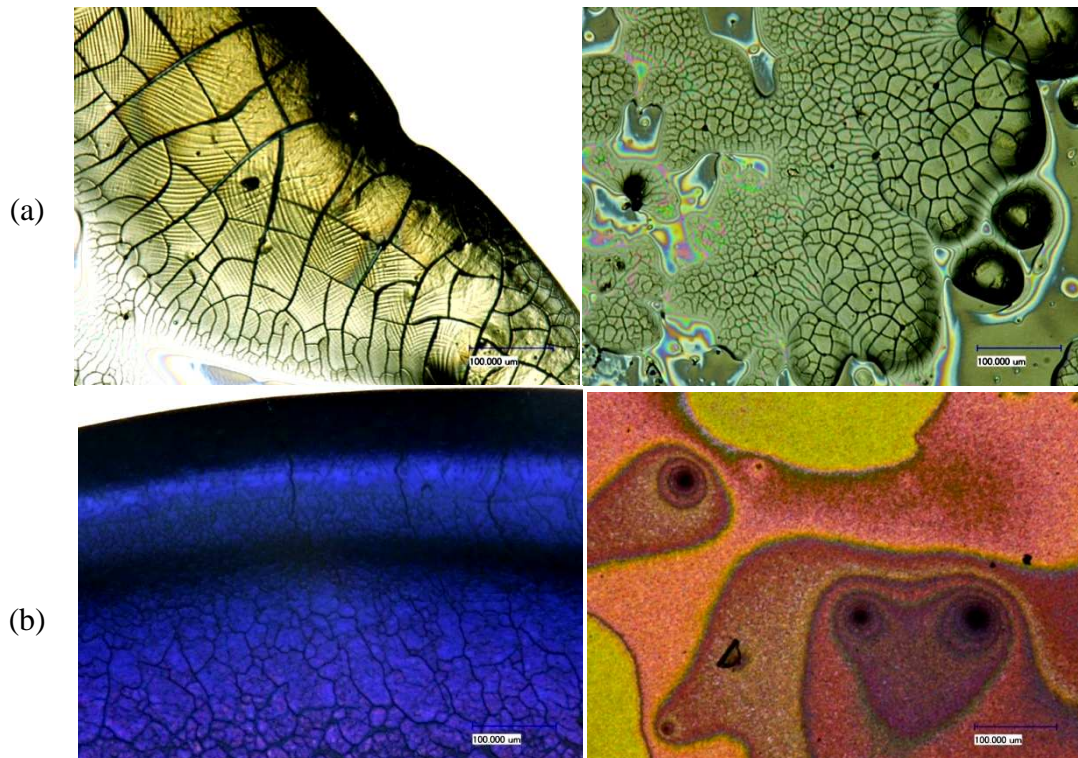


Figure 4 The selected x500 magnification optical micrographs in both rim and middle of the final dried droplets from the 10 mg/ml colloidal polystyrene solutions with (a) particles size 96 nm in comparison to (b) particles size 384 nm on the Si substrates which were only cleaned by isopropanol and acetone

According to the recorded video files of the drying of colloidal polystyrene solutions on various surfaces of Si substrates, the different drying kinetics process on the hydrophilic and the hydrophobic surfaces of Si substrates can be observed. Using the hydrophilic Si substrates in both with and without the native silicon oxide layers on top of the surfaces, the transportation of the particles due to the convective flow and the follow-up drying from the center to the periphery of the droplet can be observed. The whole drying process of 5.00 μl droplets of colloidal polystyrene solutions on top of hydrophilic Si substrate takes only 15 to 20 min depending on the room temperature. The final dried droplets as shown in Figure 5(a) and 5(b) indicate the line structural patterns at the rim of the droplets. However, the drying of colloidal polystyrene droplets on top of hydrophobic Si substrates considerably shows the different drying process. The gradual shrinkage of the droplets, the aggregation of colloidal polystyrene particles and the random flow of the particles before the droplets completely dried, can be investigated. The whole drying process of 5.00 μl droplets takes about 90 min. The line structural patterns as shown in Figure 5(c) can be observed in the position where the colloidal polystyrene particles aggregate. Therefore, the different polystyrene thin films can be produced by controlling the preparative parameters.

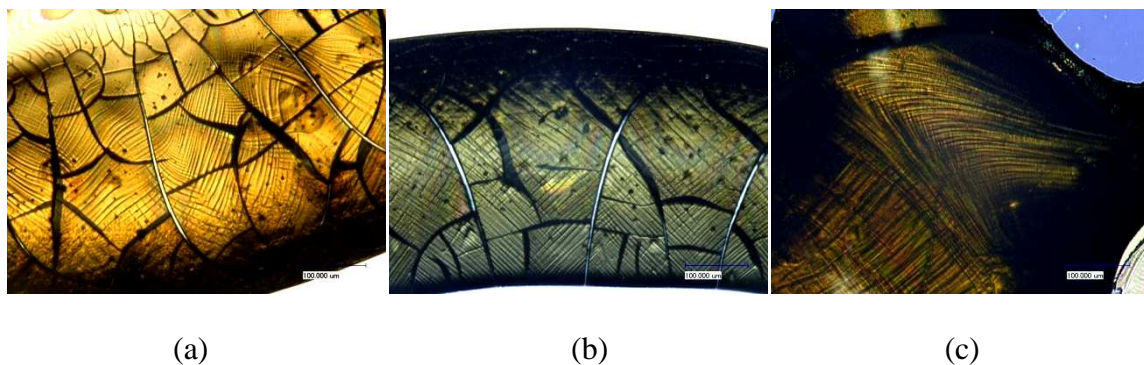


Figure 5 The selected x500 magnification optical micrographs of the rim of final dried droplets from the 25 mg/ml colloidal polystyrene solutions with particles size 96 nm on the Si substrates which were cleaned by (a) only isopropanol and acetone (b) HF solutions and (c) the Si substrate which coated the surface by polystyrene film

The interesting droplets, which formed the homogeneous areas in the middle of the droplet of sample LB6PS39 and the line structures at the rim of the droplet of sample LB2PS11 as observed from optical micrographs in Figure 6, were selected to GISAXS measurements.

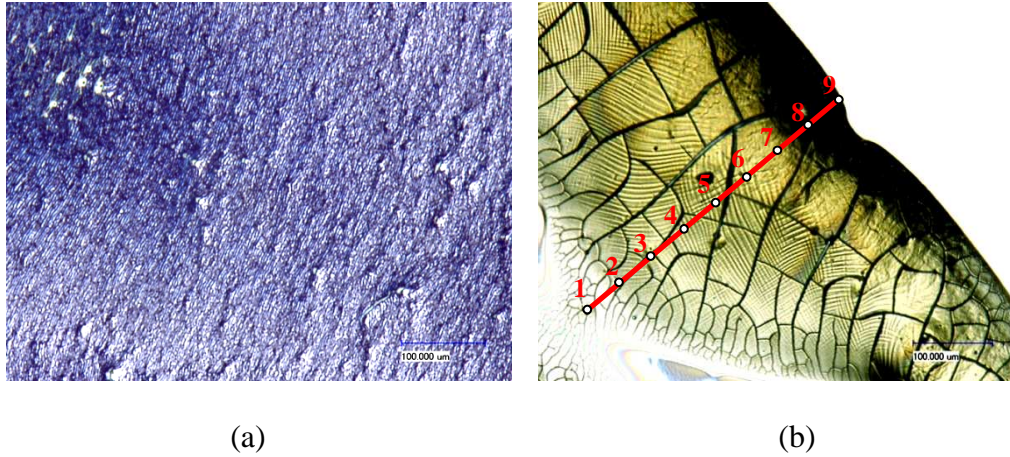


Figure 6 The x500 magnification optical micrographs of the selected droplets for GISAXS measurements of samples (a) LB6PS39 and (b) B2PS11 with the points of GISAXS scanning

3.2 GISAXS

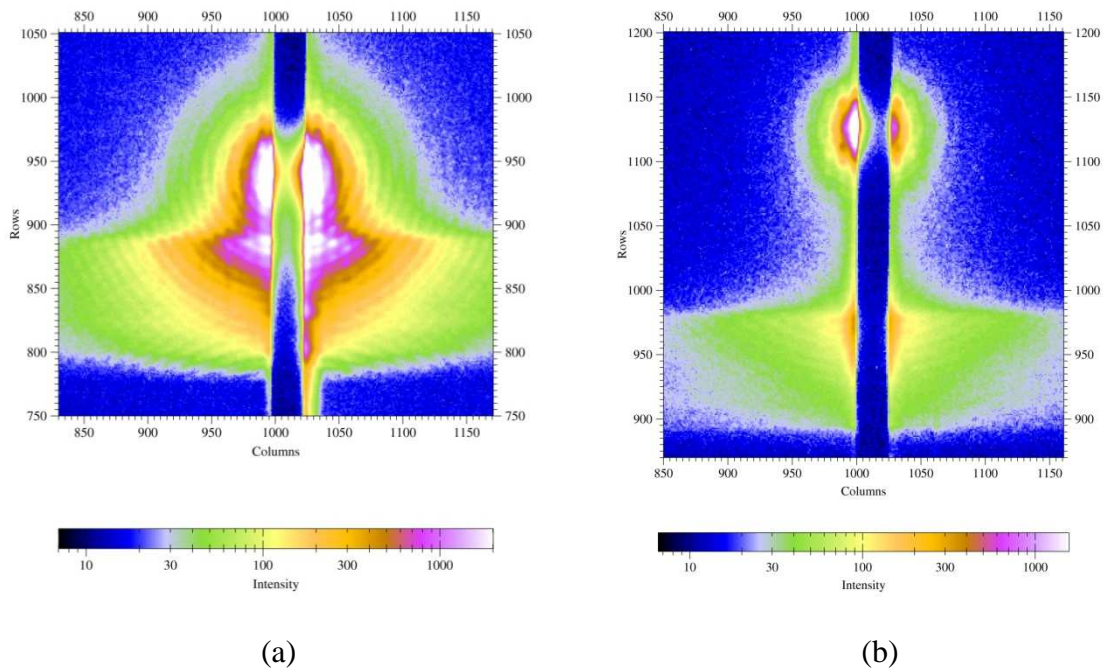


Figure 7 The two-dimensional GISAXS data of sample LB6PS39, using different incident angle (a) $\alpha_i=0.3^\circ$ and (b) $\alpha_i=0.5^\circ$

The resulting two-dimensional GISAXS data from the middle of the LB6PS39 droplets show in Figure 7. High intensity is marked in white, low intensity in blue on a logarithmic scale. The rod-like beamstop is shadowing the specular peak. Increasing of incident angle from $\alpha_i=0.3^\circ$ (Figure 7(a)) to $\alpha_i=0.5^\circ$ (Figure 7(b)), results in a large separation of specular peak and Yoneda peak. The two-dimensional GISAXS data at incident angle $\alpha_i=0.3^\circ$ is selected to study the out-of-plane cuts and the vertical cuts.

The out-of-plane cut at the exit angle equal to the critical angle of polystyrene or the row pixel position at $Y=880$ ($\alpha_c=0.138^\circ$) is illustrated in Figure 8. Figure 8(a) illustrates the corresponding intensity as a function of detector pixel positions and also indicates the Yoneda peak of polystyrene. The scattered intensity is symmetric with respect to the center. Figure 8(b) shows the corresponding intensity as a function of out-of-plane angle (ψ). The reciprocal space representation as shown in Figure 8(c) indicates the corresponding intensity as a function of scattering vector component q_y (scattered plot) in comparison to the form factor of spherical particle radius of 190 nm (line plot). The peak oscillations in the out-of-plane cut can be mainly investigated due to the form factor of spherical particles. However, the fluctuation of intensity in some part of the oscillations as indicated the peaks number 1, 2 and 4 in Figure 8(c), can be assumed that is the influence of the structure factor. The detectable length scales (ξ) of a structure factor can be calculated from q_y values at the peak number 1, 2 and 4 as followed: $\xi_1=134.20$ nm, $\xi_2=79.303$ nm and $\xi_4=39.652$ nm. The relationship of the ratio of length scales can be observed as $\xi_1: \xi_2 = 1:\frac{1}{\sqrt{3}}$ and $\xi_2: \xi_4 = 1:\frac{1}{\sqrt{4}}$ which indicated the high-ordered peaks of structure factor. However, the first-ordered length scale of the structure factor is limited by the resolution and the geometric set-up.

The vertical cut from the two-dimensional GISAXS data of sample LB6PS39 at detector pixel row $X=1024$ as shown in Figure 9(a), indicates the corresponding intensity as a function of the sum of incident angle and exit angle. The zoom-in vertical cut in Figure 9(b)

indicates the specular peak (S) and the Yoneda peak (Y) of polystyrene. The thickness of thin films (d) can be calculated from two maxima adjacent peaks between the specular peak and the Yoneda peak by the equation $d = \frac{\lambda}{\sin \alpha_{f,m} - \sin \alpha_{f,n}}$. The average thickness of the polystyrene thin film is 432 ± 48 nm which is calculated from the peaks as numbering 1 to 4 in Figure 9(b). This value is corresponding to the diameter of colloidal polystyrene particles.

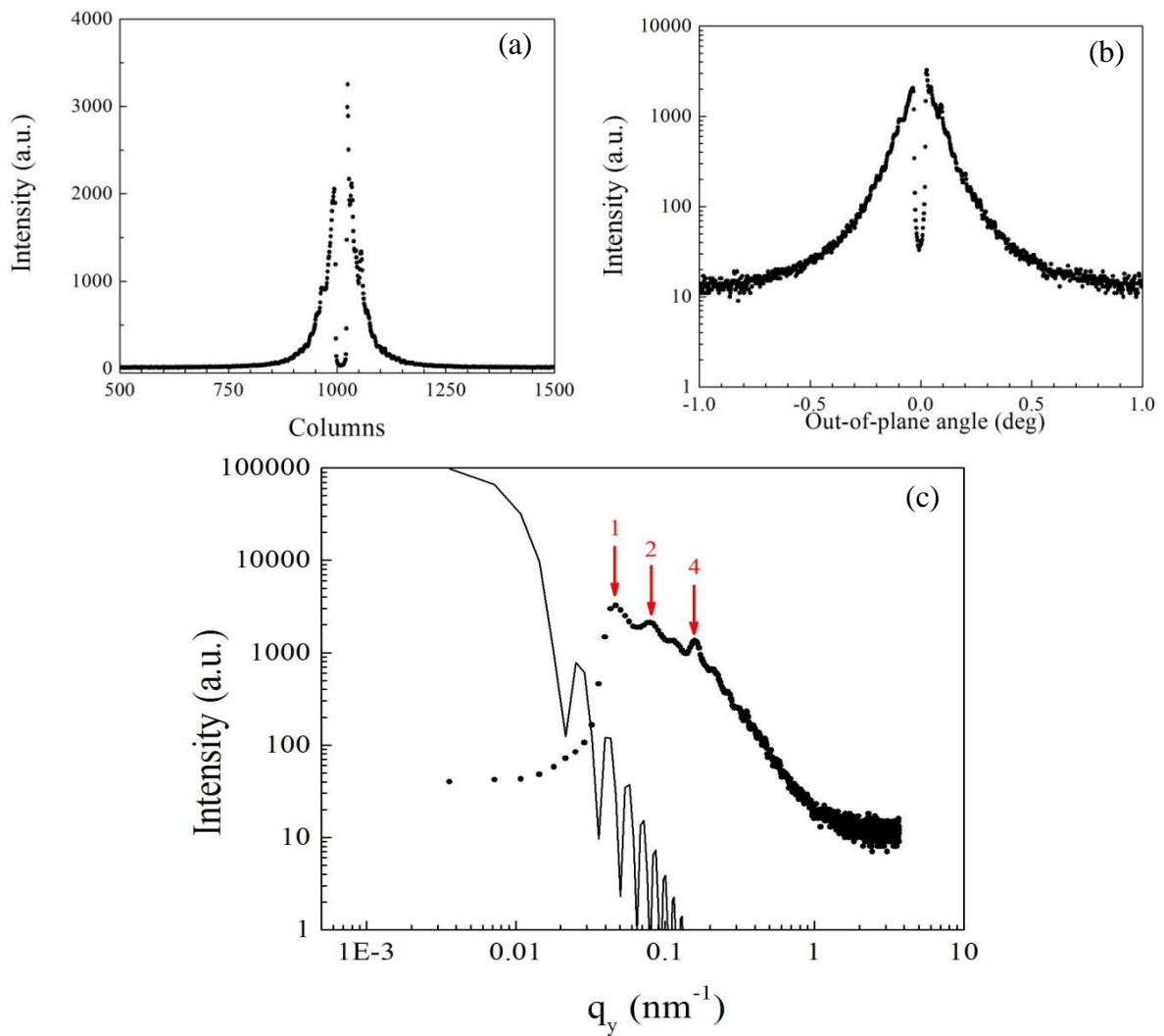


Figure 8 The out-of-plane cut from the two-dimensional GISAXS data of sample LB6PS39 at the exit angle equal to the critical angle of polystyrene which shows (a) the corresponding intensity as a function of detector pixel positions (b) the angular space representation and (c) the reciprocal space representation indicating the corresponding intensity as a function of scattering vector component q_y (scattered plot) and the form factor of spherical particle radius of 190 nm (line plot)

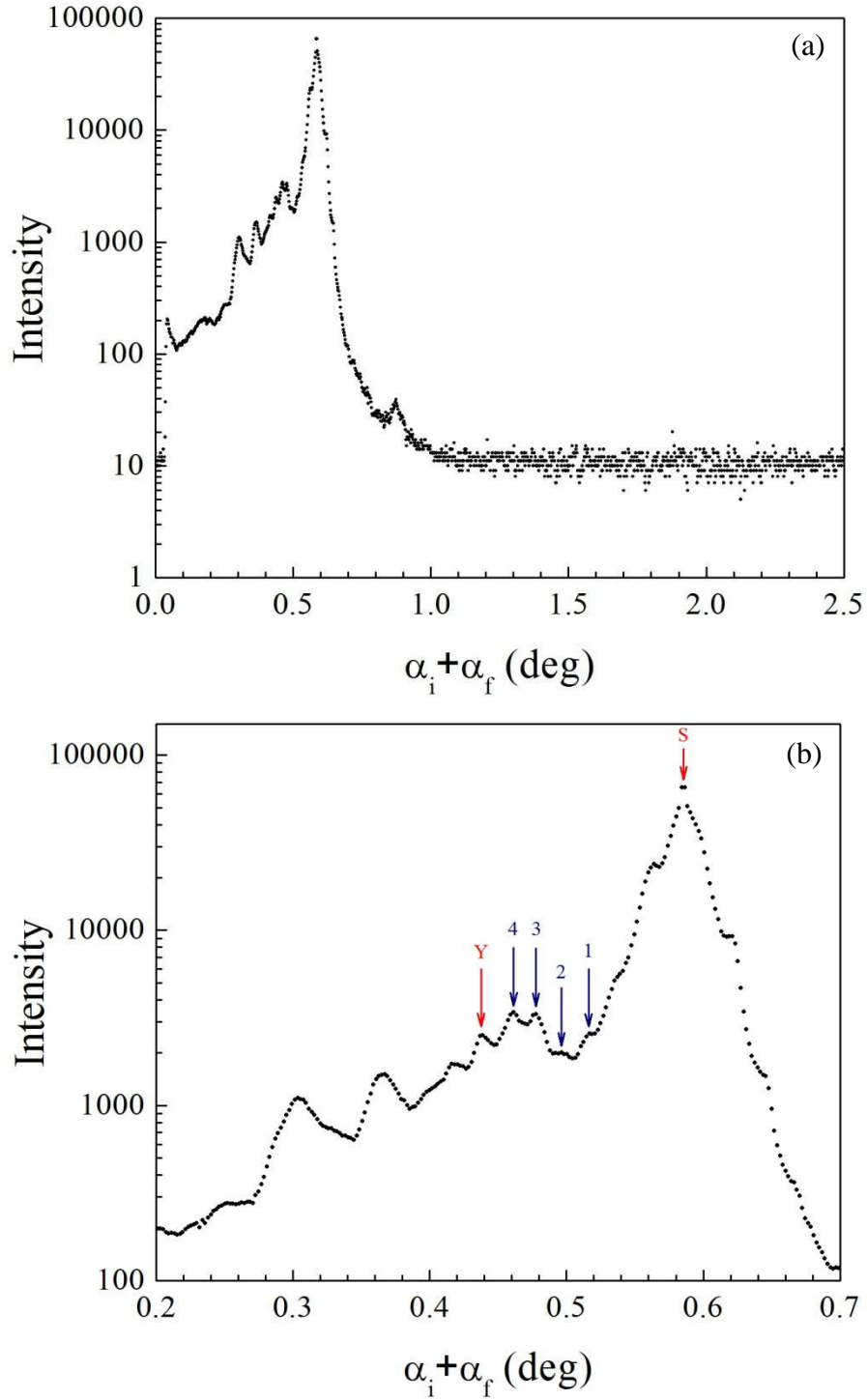


Figure 9 (a) The vertical cut from the two-dimensional GISAXS data of sample LB6PS39 at detector pixel row X=1024, which shows the corresponding intensity as a function of the sum of incident angle and exit angle (b) The zoom-in vertical cut shows the specular peak (S), the Yoneda peak (Y) and the peak position (1-4) for calculating the thickness of the polystyrene film.

The resulting two-dimensional GISAXS patterns of the line structures at the rim of sample B2PS11droplets show in Figure 10. The different patterns and intensity can be observed. At the positions which form the well-patterned line structures, the high intensity of scattering patterns can be investigated as shown in scan step number 2 to 7. However, the low intensity of scattering pattern in the last scan step can be observed from the rim position of the droplet which forms inhomogeneous film.

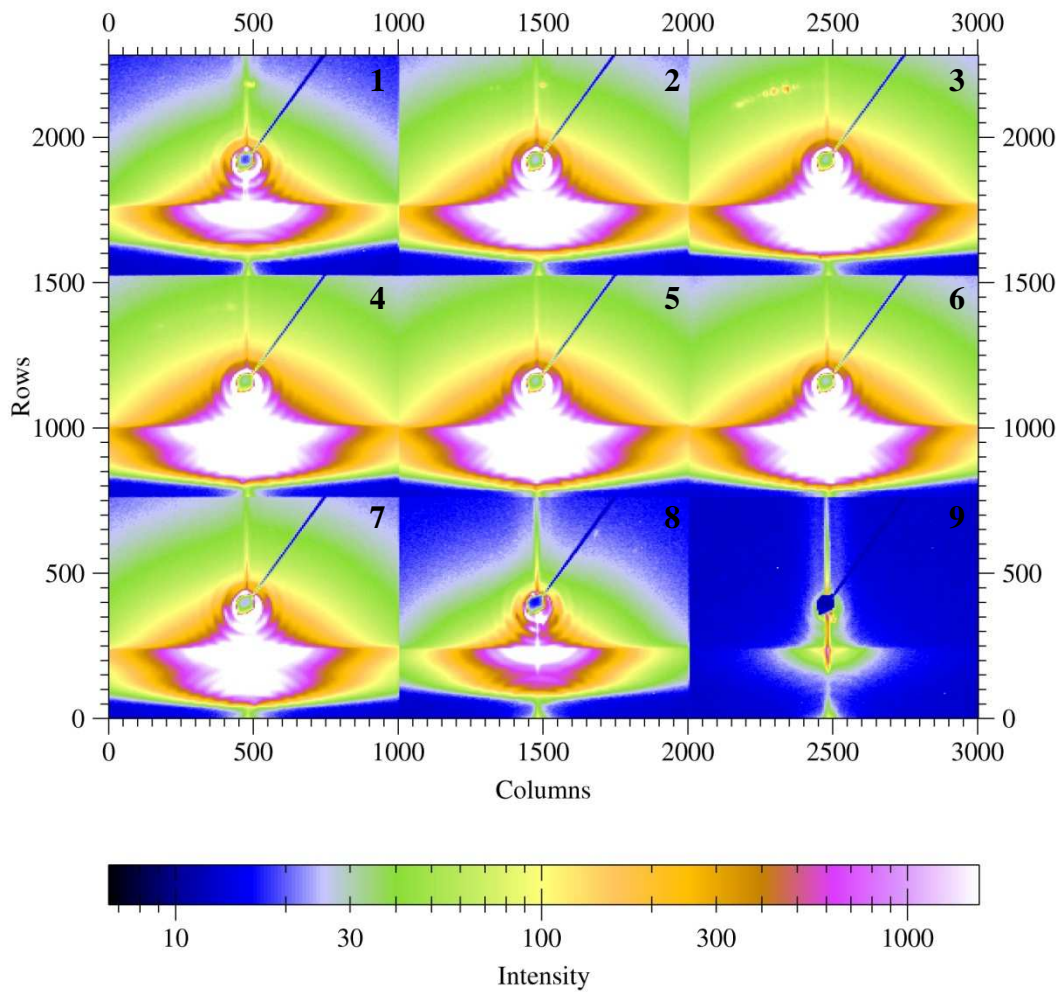


Figure 10 The two-dimensional GISAXS data of the structure at the rim of sample B2PS11 numbering from 1 to 9 which corresponding to the scan positions as shown in Figure 6(b), using incident angle $\alpha_i=0.5^\circ$ and scanning over the rim for 0.4 mm with step size $\Delta y= 0.05$ mm

4. Conclusion

The drying kinetic process of colloidal polystyrene solutions can be explained by the driving of the convective flow due to the evaporating of solvent in the droplets which therefore transports the particles and follow-up drying process from the center to the periphery of the droplet. The different patterns of polystyrene thin films can be produced by controlling the preparative parameters such as concentration, particles size and surface of substrate. The GISAXS measurements can be used to investigate the information of the structures of polystyrene thin films. The composition of form factor and structural factor of the intensity can be classified from the out-of-plane cut. The thickness of the polystyrene thin film can be calculated from the vertical cut.

5. Acknowledgements

I would like to express my special thanks and appreciation to Dr. Stephan V. Roth and Dr. Mottakin M. Abul Kashem for his supervising, valuable guidance and many kindly helps throughout the DESY summer student program. Thanks for Dr. Jan Perlich for his guidance in exercise week period. Prof. Dr. Jochim Meyer, Dr. Rainer Gehrke, Andrea Schrader and people who are behind the summer student program are also sincerely acknowledged for this invaluable experience. Furthermore, it is my great honor to be one of the Thailand representatives which passed the national selection of NSTDA and NSRC under the patronage of HRH Princess Maha Chakri Sirindhorn.

6. References

- [1] P. Siffalovic, E. Majkova, L. Chitu, M. Jergel, S. Luby, I. Capek, A. Satka, A. Timmann and S.V. Roth. *Small* (2008) DOI: 10.1002/sml.200800353.
- [2] S.A. Maier, P.G. Kik, H.A. Atwater, S. Meltzer, E. Harel, B.E. Koel and A.A.G. Requicha. *Nature Materials* 2 (2003) 229-232.
- [3] M.M. Abul Kashem, J. Perlich, A. Diethert, W. Wang, M. Memesa, J.S. Gutmann, E. Majkova, I. Capek, S.V. Roth, W. Petry and P. Müller-Buschbaum. *Macromolecules* 42 (2009) 6202-6208.
- [4] E. Metwalli, S. Couet, K. Schlage, R. Röhlberger, V. Körstgens, M. Ruderer, W. Wang, G. Kaune, S.V. Roth and P. Müller-Buschbaum. *Langmuir* 24 (2008) 4265-4272.
- [5] G. Renaud, R. Lazzari, C. reventant, A. Barbier, M. noblet, O. Ulrich, F. Leroy, J. Jupille, Y. Borensztein, C.R. Henry, J.-P. Deville, F. Scheurer, J. Mane-Mane and O. Frucharts. *Science* 300 (2003) 1416-1418.
- [6] G. Bauer, J. Hassmann, H. Walter, J. Haglmüller, C. Mayer and T. Schalkhammer. *Nanotechnology* 14 (2003) 1289-1311.
- [7] S.V. Roth, R. Döhrmann, M. Dommach, M. Kuhlmann, I. Kröger, R. Gehrke, H. Walter, C. Schroer, B. Lengeler and P. Müller-Buschbaum. *Rev. Sci. Instrum.* 77 (2006) 085106-1 – 085196-7.
- [8] P. Müller-Buschbaum. *Anal. Bioanal. Chem.* 376, (2003) 3-10.
- [9] P. Müller-Buschbaum, E. Bauer, S. Pfister, S.V. Roth, M. Burghammer, C. Riekkel, C. David and U. Thiele. *Europhys. Lett.* 73(1) (2003) 35-41.
- [10] E. Metwalli, J.-F. Moulin, J. Perlich, W. Wang, A. Dietert, S.V. Roth and P. Müller-Buschbaum. *Langmuir* (2009) DOI: 10.1021/la901432j.
- [11] S.V. Roth, T. Autenrieth, G. Gröbel, C. Riekkel, M. Burghammer, R. Hengstler, L. Schulz and P. Müller-Buschbaum. *Appl. Phys. Lett.* 91 (2007) 091975-1 – 091975-3.